


Correlative nanoscopy: A multimodal approach to molecular resolution

Samira Jadavi^{1,2} | Paolo Bianchini² | Ornella Cavalleri¹ | Silvia Dante³ |
Claudio Canale¹  | Alberto Diaspro^{1,2}

¹DIFILAB, Department of Physics, University of Genova, Genova, Italy

²Nanoscopy, CHT Erzelli, Istituto Italiano di Tecnologia, Genova, Italy

³Materials Characterization Facility, Istituto Italiano di Tecnologia, Genova, Italy

Correspondence

Claudio Canale, DIFILAB, Department of Physics, University of Genova, Via Dodecaneso 33, Genova, Italy.
Email: canale@fisica.unige.it

Funding information

DIFILAB, Grant/Award Number: RBAP11ETKA-005; Programmi di Ricerca Scientifica di Rilevante Interesse Nazionale (PRIN). MIUR, Grant/Award Number: 20177XJCHX_003

Review Editor: adi salomon

Abstract

Atomic force microscopy (AFM) is a nano-mechanical tool uniquely suited for biological studies at the molecular scale. AFM operation is based on mechanical interaction between the tip and the sample, a mechanism of contrast capable of measuring different information, including surface topography, mechanical, and electrical properties. However, the lack of specificity highlights the need to integrate AFM data with other techniques providing compositional hints. In particular, optical microscopes based on fluorescence as a mechanism of contrast can access the local distribution of specific molecular species. The coupling between AFM and super-resolved fluorescence microscopy solves the resolution mismatch between AFM and conventional fluorescence optical microscopy. Recent advances showed that also the inherently label-free imaging capabilities of the AFM are fundamental to complement the fluorescence images. In this review, we have presented a brief historical view on correlative microscopy, and, finally, we have summarized the progress of correlative AFM-super-resolution microscopy in biological research.

KEYWORDS

AFM, correlative microscopy, correlative nanoscopy, STED, STORM

1 | INTRODUCTION

Most of the cell biology challenges take advantage of the augmented investigation capability provided by the increased resolution offered by microscopy. Starting from the XVII century, microscopy has been synonymous with optical microscopy, that is, with the use of lenses to deviate light to produce a magnified image. In the twentieth century, new techniques able to reach and overcome resolutions at the nanometer scale enriched the microscopy world. In particular, electron microscopy (Kruger, Schneek, & Gelderblom, 2000), developed in 1933, has made significant contributions in various fields of science while remaining limited to the study of samples in a specific environment, that is, in vacuum, a condition that is far from the physiological

environment. A new machine version, called environmental electron microscope (Swift & Brown, 1970), has been developed and applied to the study of samples at atmospheric pressure and humidity. Still, it was not wholly won: it is impossible to observe live samples, or dynamic molecular processes with electron microscopy techniques. The scenario changed in 1986, the year in which the first atomic force microscope (AFM) was presented (Binnig, Quate, & Gerber, 1986).

AFM is a whole set of tools capable of doing a comprehensive study of bio-mechanisms, such as the self-assembly of molecules (Di Gaetano et al., 2006), or bio-samples properties, such as the morphological and mechanical properties of cells and tissues (Bellani, 1971–1983 (2014); Mescola et al., 2012). The combination of measuring forces with a high spatial resolution of biological samples

This is an open access article under the terms of the Creative Commons Attribution-NonCommercial License, which permits use, distribution and reproduction in any medium, provided the original work is properly cited and is not used for commercial purposes.

© 2021 The Authors. *Microscopy Research and Technique* published by Wiley Periodicals LLC.

without labeling and working near-physiological conditions makes AFM unique (Doss et al., 2020). Despite this wide range of demonstrated abilities, this technique alone does not allow the specific identification of individual elements of a heterogeneous sample due to the lack of chemical specificity. This limitation could be restrictive in the study of crowded molecular environments, such as cells or biomembrane. Furthermore, the AFM is a surface technique that cannot access the inner region of a three-dimensional sample, such as a cell.

Fluorescent light microscopy is an advanced part of light microscopy that enables the recognition of specific component/components inside a heterogeneous sample with very high specificity (Sanderson, Smith, Parker, & Bootman, 2014). In this technique, a fluorophore is first excited by an excitation light, and then it decays nonradiatively toward a lower metastable state. From this state, spontaneous emission, or fluorescence occurs. The fluorophore again goes back to the ground state, emitting a photon with the same energy of the gap between the two states (spontaneous emission). The diffraction of light limits the resolution of optical microscopy. In 1873, Ernst Abbe, first described the diffraction limited resolution of a microscope as the ability to distinguish two objects separated by distance $d = \lambda/2n\sin\theta$, where λ is the wavelength of light and $n\sin\theta$ is the numerical aperture (NA) of the objective lens (Sheppard, 2017). These days, most oil objectives have a maximum NA of 1.25, meaning that the maximum resolution of a light microscope is limited to around 250 nm that is far from the scale at which molecular processes occur and not compatible with the distance between molecules in a crowded environment such as the cell. However, Eric Betzig, in 1995, published a theoretical paper on the idea of using population-based localization methodologies. In this paper, the author suggested that it is possible to reduce all the fluorophores into single spots over time, by individually turning the fluorophores on and off (Liu, Lavis, & Betzig, 2015). William Merlin, in 1997, by publishing an article entitled "On/off blinking and switching behavior of single molecules of green fluorescent protein" paved the way for Betzig to find the next piece of the puzzle (Dickson, Cubitt, Tsien, & Moerner, 1997). Finally, in 2006, three techniques, known as stochastic optical reconstruction microscopy (STORM), photoactivated localization microscopy (PALM), and fluorescence PALM were introduced to achieve subdiffraction limit resolution (Hess, Girirajan, & Mason, 2006; Rust, Bates, & Zhuang, 2006). The idea behind these switching based techniques is to stochastically activate a few fluorophores in time to resolve single molecules between activated and dark states. Therefore, with randomly shining an activation laser on a specimen, only a small subset of fluorophores has the chance of being photoactivated at each time step. In this case, the images are acquired over a few frames until the target fluorophore switches back into the dark state or becomes photobleached. However, long integration times to get enough photons for achieving the high desired localization accuracy is a limiting factor regarding these techniques. Another approach toward super-resolution microscopy was already suggested by Hell and Wichmann (1994): the concept of stimulated emission depletion (STED) microscopy. The trick is to prevent the spontaneous emission by having an additional depletion laser. This depletion light, is designed such that, instead of the fluorescent, or spontaneous emission, it will lead to stimulated emission at a wavelength significantly different from the

fluorescence wavelength (Hell & Wichmann, 1994). The depletion laser, also called STED beam, features a zero intensity region at the center. In this way, most of the molecules in the STED beam region are switched off and only fluorophores located at the periphery (i.e., the center) of the excited region can be stimulated by a second beam to emit fluorescence. By playing this on-off game, details of a biological sample as small as 20–30 nm can be resolved, which accounts for an approximately 10-fold improvement in resolution over traditional fluorescence microscopy. Although fluorescence microscopy techniques can simultaneously identify several specific components and deeply visualize a cell, they cannot characterize all the products derived from the cell structure. Indeed, the labeling process in fluorescence microscopy is functional, meaning that the fluorescent probes only tag specific parts of the biological sample. As a result, in fluorescence microscopy, we can only see what we have decided to image. This statement reveals the importance of correlating fluorescence data with others derived from label-free techniques. This loss of information affects both the imaging and the spectroscopic techniques based on the use of fluorescence, suggesting a primary role for correlative techniques.

Correlative microscopy is an approach that combines the imaging capabilities of different microscopy platforms in one instrument to provide information that one or the other microscope alone cannot. Correlative microscopy has many different approaches to get back and forth between the devices and different probe approaches. Exploiting correlative information makes it possible for researchers to understand the complicated relationship between structure and function by visualizing functional information in the context of structural information in biological research. With this motivation, the first STED-AFM coupled system took shape in 2012 (Harke, Chacko, Haschke, Canale, & Diaspro, 2012). A combination of AFM with a super-resolution microscopy system such as STED generates a nanoscopic tool with very high versatility to answer subdiffraction level morphological questions. Furthermore, the two techniques can also integrate different information combining them in different ways. The AFM topography, for example, can be coupled with spectroscopic optical data, the fluorescence imaging can be boosted by the coupling with high-resolution mechanical data.

However, the story of optical-scanning Probe correlative microscopy was started a couple of decades in advance with the first pioneering, although rough, approaches. In this review, we will present a brief historical view on correlative microscopy, and, finally, we will summarize the progress of correlative AFM-super-resolution microscopy techniques in biological research.

2 | CORRELATIVE AFM-OPTICAL FLUORESCENCE MICROSCOPY. A HISTORICAL OVERVIEW

2.1 | Pioneering attempts

AFM and fluorescence light correlative microscopy is a platform based on the direct overlay of images acquired with AFM and light microscopy. The idea to couple the AFM with the optical microscopy

rose right after the first application of the AFM on bio-samples (Hansma, Elings, Marti, & Bracker, 1988). Initially, the optical microscope was thought to be a tool for identifying a particular structure and choosing the area for the AFM inspection, particularly useful in cell imaging. This point was essential, since the positioning of the AFM probe on the object of interest by subsequent image acquisition was very time-consuming, mainly when the sample was randomly distributed on the substrate and not very dense. The second issue of this method was related to the high probability of tip contamination, or damage in the first preparation phase. Another fundamental idea was to enrich the AFM analysis with other important information from the same area, derived, for example, by using fluorescence microscopy. Two different attempts to reach these goals were presented in 1992. Radmacher, Eberle, and Gaub (1992) introduced an AFM system with an integrated long-distance objective, able to image the sample in an upright configuration, also in fluorescence mode (Figure 1a). This solution was dictated by the configuration of the first AFMs that were generally sample scanning systems. The limitation of this setup was the poor magnification associated with the use of an objective with a working distance of several centimeters. The resolution of the optical system, around $3\ \mu\text{m}$, far from the resolution of molecular processes, was not enough to correlate the fine details of the AFM imaging. In the same year, Putman et al. (1992) proposed an original solution to couple optical lenses in an inverted configuration, acquiring a reflection image from below, using a transparent substrate to mount the sample. In this work, a small lens is mounted directly in the free space of a typical piezo-tube with a hollowed cylinder geometry (Figure 1b). The resolution was close to $1\ \mu\text{m}$, but the system had a complicated design, not ideal for further developments.

Just 1 year later, in 1993, the same group presented a new system. Taking advantage of the recent development of head-scanning

AFM, a commercial inverted optical microscope was coupled with the AFM (Putman, van Leeuwen, de Groot, Radosevic, & Greve, 1993). The lack of the piezo scanner between the scanner and the sample allowed this new solution that will be preferred for the most advanced application in the following. The objective approaches the transparent substrate without any steric constriction. Furthermore, the optical path from the objective lenses to the sample is free, while using a telescope from the top, the AFM probe is between the lenses and the sample precluding the sample view in the correspondence of the AFM tip. For the first time, the author employed a confocal laser scanning microscope (CLSM) (Jonkman, Brown, Wright, Anderson, & North, 2020). The advantage of CLSM is related to its capability to study the inner part of the cell in details. CLSM can define the optical plane of acquisition, having the potential to characterize the internal part of the cell with a better signal to noise ratio, being able to distinguish the structures that are present at the basal plane at the mid-plane, or the apical plane of the cell. This possibility is precluded in the AFM. The quality of the correlated images increased with respect to the previous works.

A similar design was also proposed by Henderson and Sakaguchi (1993) just a few months later, integrating a commercial inverted optical microscope to a head-scanning AFM, at least in part commercially available (Figure 1c). In their work, Henderson et al. showed for the first time the correlation between single cells and cell compartments visualized by AFM and optical microscopy. Although using a far-field fluorescence microscope, by selectively labeling the F-actin with rhodamine-phalloidin and using a $\times 100$ oil immersion objective, Henderson et al. were able to image the actin filaments with the optical microscope and correlate this signal with the AFM topography. The basis of correlative AFM-optical microscopy was built, paving the avenue for future developments.

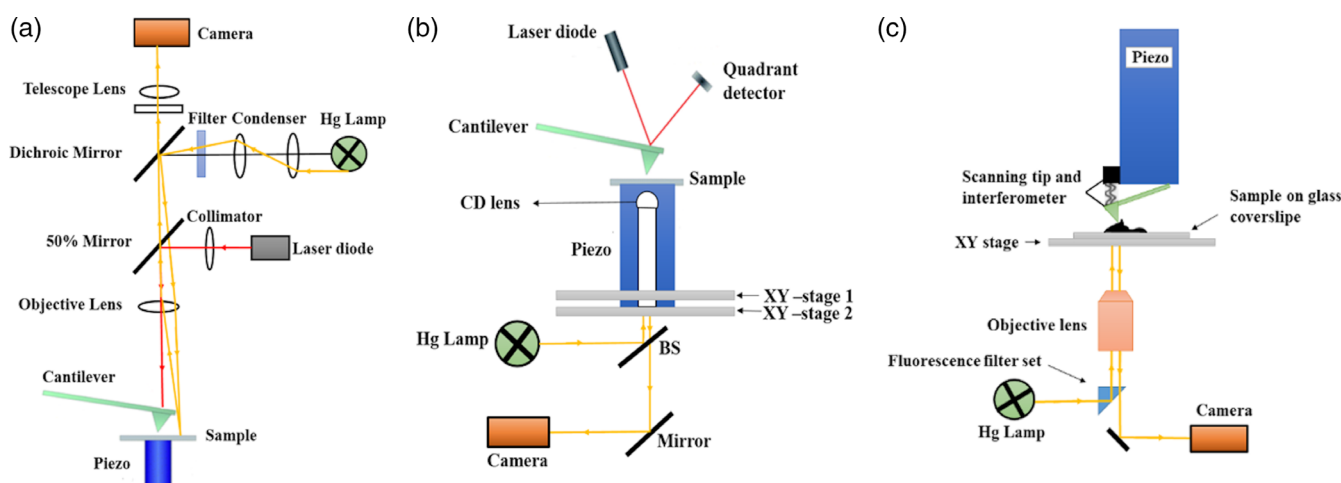


FIGURE 1 The first integrated system proposed by Radmacher et al. was based on the use of a long distance objective to focus the sample at a distance that was higher than the scanner thickness (a). A lens integrated on the piezo-actuator was used by Putman et al. to visualize the sample from its bottom side (b). The use of head-scanning atomic force microscopy (AFM) systems allowed the use of standard inverted optical microscopes (c). The solution here represented in (c) has been the most successful, especially in the study of bio-samples

2.2 | Significant improvements

Dvorak and Nagao (1998) presented an integrated system that simultaneously acquired correlated images in AFM, bright field, epifluorescence, and surface interference microscopy modes (Tychinsky & Tikhonov, 2010; Verschueren, 1985), achieving the highest level of integration obtained until that time. In particular, the optical system was based on a custom developed set-up able to exploit transmitted oblique, reflected fluorescence, and reflected interference microscopy acquired simultaneously with AFM scan. The instrument was equipped with a new thermostat to control the cell culture environment, a fundamental component that maintains the optimal condition for living cell analysis minimizing the cantilever drift. Correlated bright field, epifluorescence, surface interference microscopy images of bovine embryonic skin, and muscle (BESM) cells were shown in correlation with the AFM scans (Figure 2). The combination of surface interferometry microscopy and AFM provided information on the relationship between the cell and the substrate and the global three-dimensional topography of the cell. The authors also applied the technique to BESM cells infected with a toxic agent, the protozoan parasite *Toxoplasma gondii* (*T. gondii*) (Dubremetz, 1998). In particular, they used for the first time AFM in force volume imaging mode (Medalsy, Hensen, & Muller, 2011; Seghezze, Dante, Diaspro, & Canale, 2015) under controlled environmental conditions coupled with transmitted bright field and tapping mode AFM imaging. Bright-field imaging (Figure 2a) revealed the internal contents of the cell allowing the localization of organelles and parasites. Tapping mode AFM imaging (Figure 2b) showed the surface topography of the cell, but also mapped the distribution of the cytoskeleton fibers located in the proximity of the apical part of the cells. Force volume (Figure 2c) demonstrated that the internal content defines the local mechanical properties of the cells, and the presence of the *T. gondii* leaves a characteristic footprint in the elasticity map. The last finding had fundamental importance since it indicated that the technology was ready

for advanced nano-mechanical characterization of bio-samples (Garcia-Manyes, Redondo-Morata, Oncins, & Sanz, 2010; Seghezze et al., 2015).

The quality of the correlated AFM-far field optical microscopy imaging improved quickly. Despite this, the method generally followed for spatial correlation in far-field optical microscopy-AFM was still based on the manual positioning of the AFM tip on the sample region of interest, looking at the AFM probe and sample with an optical microscope. In a second fine-tuning, the AFM scan parameters were optimized until the region of interest was precisely located under the AFM probe. This approach provided effective results, but only in the analysis of sample features large enough to be visualized by low NA optical lenses, such as the whole biological cells, or their prominent organelles (e.g., the nucleus) (Ferrera et al., 2014). Smaller objects are clearly distinguished in optical microscopy only by employing high-magnification and high-NA microscope optics, making challenging proper positioning of the probe due to the several restrictions imposed by the use of high performances objectives. The cantilever is often out of focus, being outside of the depth of field of the optical system. Furthermore, the precise position of the AFM tip is not easily detectable. These drawbacks hinder the ability to correlate the AFM and optical images at the nanoscale level; in the first applications, the sample features under examination were necessarily in the range from several hundreds of nanometers to micrometers.

Kolodny, Willard, Carillo, Nelson, and van Orden (2001) achieved a significant improvement exploiting the integration between an AFM and an optical microscope to correlate the AFM topographical signal with local fluorescence spectroscopy data. In particular, the authors proposed an original method to combine time-resolved fluorescence measurement (Ross & Jameson, 2008) and AFM, correlating the spectroscopic and topographical data. The light of the confocal laser beam scattered by the AFM tip during the scan was observed to achieve this goal. The image of the light scattered by the AFM tip, overlapped with the AFM topography, allowed for an unambiguous determination

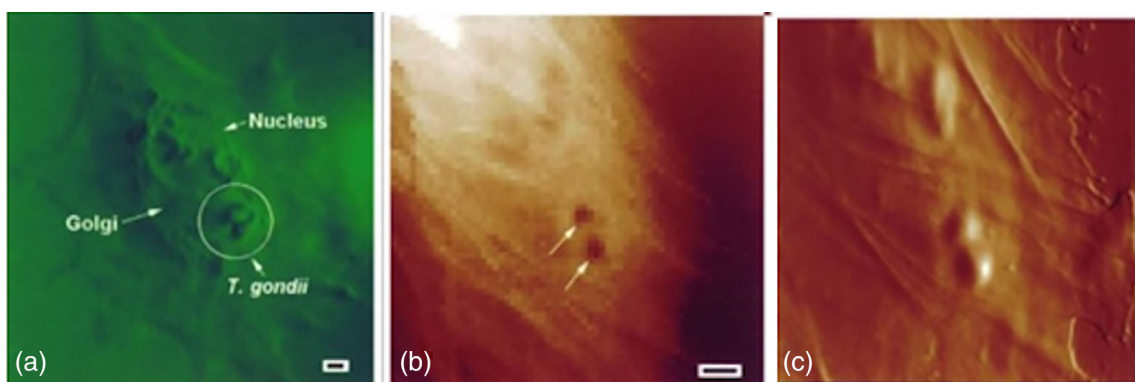


FIGURE 2 Concurrently collected bright field optical image of a *T. gondii*-infected bovine embryonic skin, and muscle (BESM) cell (a). Tapping mode amplitude image on the same area give a qualitative view of the morphological features characterizing the cell surface (b). The presence of an increased stiffness in the correspondence of the parasites is demonstrated in the force-volume map shown in (c). We must note that darker color have been chosen to represent the stiffer portion of the sample, in the following, an opposite convention was generally used (stiffer area are brighter than the softer). The circle in (a) and the arrows in (b) represent the same area. Scale bar: 10 μm . Modified from Dvorak and Nagao (1998)

of part of the sample positioned within the optical microscope's excitation region. The authors applied this technique to fluorescently labeled DNA and fluorescent polystyrene nano-beads molecules dispersed on mica (Figure 3). The approach proposed in this work represented a significant step toward the application of combined far-field optical microscopy-AFM to the study of individual nanosized object. It was clear that the integration between AFM and optical microscopy could be not only a tool for advanced imaging, but could also provide a new perspective in the correlation of plenty of physical quantities that changes locally, even at the nanoscale. Although the way toward high-resolution correlative microscopy was opened for some years, most of the applications were still on microsized objects, and in some cases, the correlation between AFM and optical signals were achieved indirectly by using substrates with markers to identify the portion of the sample of interest (e.g., cells) performing AFM and optical microscopy separately on two different setups. For example, Haga et al. (2000), using this approach, demonstrated the important contribution of intermediate filaments and actins in the definition of fibroblast cells elastic properties). They also showed that tubulin concentration is scarcely influencing cell elasticity. To reach this goal, they acquired force volume maps on living fibroblasts by using a commercial AFM. The samples were fixed right after the AFM analysis and stained for immunofluorescence imaging. The sample was moved on the confocal microscope, and the same cells mapped by AFM were imaged. The use of markers on the coverslip to identify the single cells under analysis was not declared in the manuscript; however, it is clear

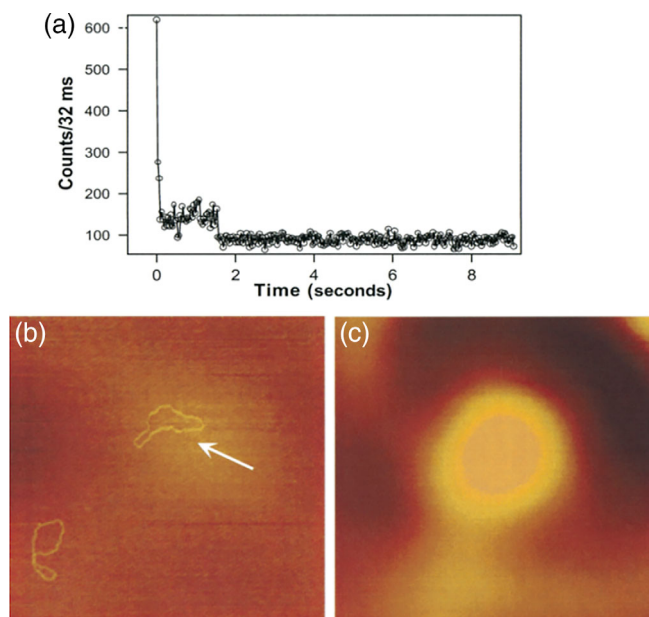


FIGURE 3 (a) Time-resolved fluorescence measurement observed from labeled DNA molecules using a 32-ms time bin for fluorescence counts. (b) Sample topography imaged by atomic force microscopy (AFM) with a height scale of 3 nm. (c) The bright spot shows the scattered light of the PSF of the optical microscope. The arrow in image (b) indicates an individual DNA molecule related to the PSF in image (c). The image sizes are $1.80 \times 1.80 \mu\text{m}^2$. Figure from Kolodny et al. (2001)

that the correlation between large images with an area of $80 \mu\text{m}^2$ is satisfactory also by using this indirect method that does not imply a specific work on the setup. The manuscript of Kondra et al. (2009) demonstrated again that the indirect correlation of confocal light microscopy and AFM images could provide new insight on the biological sample. In this work, the superimposition between images acquired by using different technique and by acquiring images with different file format, resolution, and so forth, was achieved and optimized taking advantage of tools used in computer vision (Trucco & Verri, 1998). In particular, by employing custom-made substrates for cell culture with markers for cell recognition, the growth cones of neural cells were observed in two subsequent steps by CLSM and AFM. The cells were analyzed after fixation. Different molecules were specifically labeled, enabling the fluorescence imaging of the confocal images neuronal Class III-tubulin, neural cell adhesion molecule or F-actin. The AFM scans provided a high-resolution 3D image of the same structure, perfectly correlated with the optical image.

2.3 | The advent of super-resolution

2.3.1 | AFM-STED

Harke et al. (2012) reported the combination of different AFM modes with the super-resolution STED microscopy. A nominal multiphoton fluorescence microscope equipped with a custom-made STED microscope was supplemented with AFM. Initially, the main aim was to provide chemical specificity to the AFM, by coupling it with a fluorescence technique with a comparable lateral resolution. The choice of STED microscopy, among all the available super-resolution techniques was suggested by the unique capability of STED such as fast image acquisition (in particular if compared with the slow acquisition rate of the AFM), the possible integration with other fluorescent-based techniques as fluorescence correlation spectroscopy (Eggeling et al., 2009), fluorescence lifetime imaging (Wallrabe & Periasamy, 2005), fluorescence recovery after photobleaching (Rayan, Guet, Taulier, Pincet, & Urbach, 2010), and so forth. As a first test sample to check the platform performance, fluorescent spherical beads with specified diameter of 40 nm were measured under dry conditions. The results shown in Figure 4b,d represented single fluorescent beads in STED image and in topographical AFM of the same area of interest, respectively. It was possible to associate each single feature displayed by AFM with the fluorescent trace in the STED image. On the contrary, the confocal image (Figure 4a) showed only blurred fluorescent spots in which the trace of the single beads was lost. From the results, they pointed out that the targeting capability of STED technique is compatible with that of the AFM, but is enriched with chemical specificity, and this confirmed STED as an ideal candidate to improve AFM analysis.

As a second test sample, the labeled microtubules of cos7 cells were measured under aqueous conditions. Also in this case, the confocal data could not confirm the AFM data, whereas the number of the microtubules was clearly distinguished from the rest of the cell

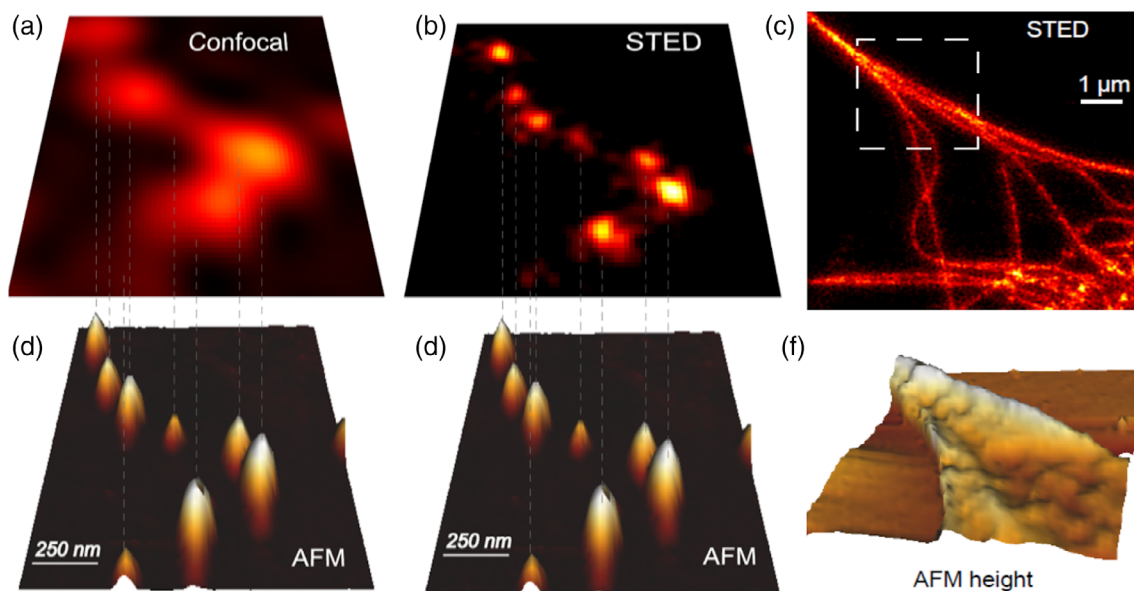


FIGURE 4 (a,b) Confocal and stimulated emission depletion (STED) images of fluorescent spheres of 40 nm size, respectively. (c) STED image of fluorescently-labeled microtubules in cos7 cells (d–f) 3D rendered view of height analysis extracted from atomic force microscopy (AFM) images of (a–c), respectively. Part of the figure was modified from Harke et al. (2012)

area in the images acquired with STED (Figure 4c). The AFM force maps of an area of interest were acquired to extract the Young's modulus gaining information about the cell stiffness. The Young's modulus map matched with the data extracted from the STED images suggesting interesting application in nanomechanics (data not shown). The higher precision given by STED microscopy also reduced the total number of force spectroscopy cycles for the adhesion determination which thereby reduced the risk of possible tip contamination.

The ability to see objects with STED at a comparable (if not with the same) lateral resolution given by AFM motivated the same authors to move to nano-manipulation using AFM–STED. AFM itself is a nano-manipulator. It can push on a particular position of the sample with a very well defined force, move nanosized objects, stimulate mechanically a living cell, or modify a biological specimen (Di Bucchianico et al., 2011). All these operations are very time-consuming and sometimes invasive if the manipulation path is defined from a previously acquired AFM image. The AFM is slow, and the position of the sample can change due to sample dynamics or simply to thermal drift resulting in a significant source of indeterminateness, especially when the target has a size in the order of the nanometer. Furthermore, on extremely soft and delicate samples such as cells, the AFM imaging is not providing high lateral resolution, and the prolonged interaction between tip and cells can damage the sample itself. The use of a high-resolution STED image to identify the position and trajectory followed by the AFM probe appears a very promising solution. Noninvasive STED imaging provides the coordinates to precisely move the AFM tip. Furthermore, in a heterogeneous sample, the system is provided of chemical specificity. The authors manipulated 40 nm fluorescent beads, moving them along a line with a total displacement around 150 nm (Figure 5) (Chacko, Canale, et al., 2013).

The bead movement was followed by acquiring two STED image before and after the manipulation (Figure 5a–c). An intriguing idea was to follow the effect of the interaction between tip and sample in real time by fast acquisition of subsequent STED images. This application could be very important in field such as nanosurgery. The authors noted that this operation is possible, but during manipulation, the STED image cannot be acquired at the maximum resolution allowed by the super-resolution setup. In fact, STED resolution depends on the intensity of the laser employed to induce stimulated emission (the depletion beam). When the silicon/silicon nitride tip is in contact with the sample, that is, is positioned exactly in the optical focus, the high intensity laser reflected by the tip damages the sample, and in some cases, also the AFM probe. For this reason, after choosing the trajectory for the manipulation from high resolution STED images, the dragging of the beads was observed at a lower resolution reduced the power of the STED laser from 200 to 50 mW (see Figure 5d). Two images acquired with an STED laser power of 300 mW are shown in Figure 5e,f.

The next step in targeted manipulation was the manipulation in a liquid environment. In 2014, for the first time, Chacko, Harke, Canale, and Diaspro (2014) proposed the concept of correlative STED–AFM-based biomanipulation in which biological samples could be manipulated in a liquid environment with discrete units of force at the single molecule level. The experiments were conducted on labeled microtubules of fixed fibroblast cells. The fast acquisition imaging time of STED–AFM was able to live monitor the quick responses of filaments movements to mechanical forces inside the cell (data not shown) (Chacko et al., 2014). This particular application is precluded by using SMLM techniques where the need of long integration time is not allowing fast visualization.

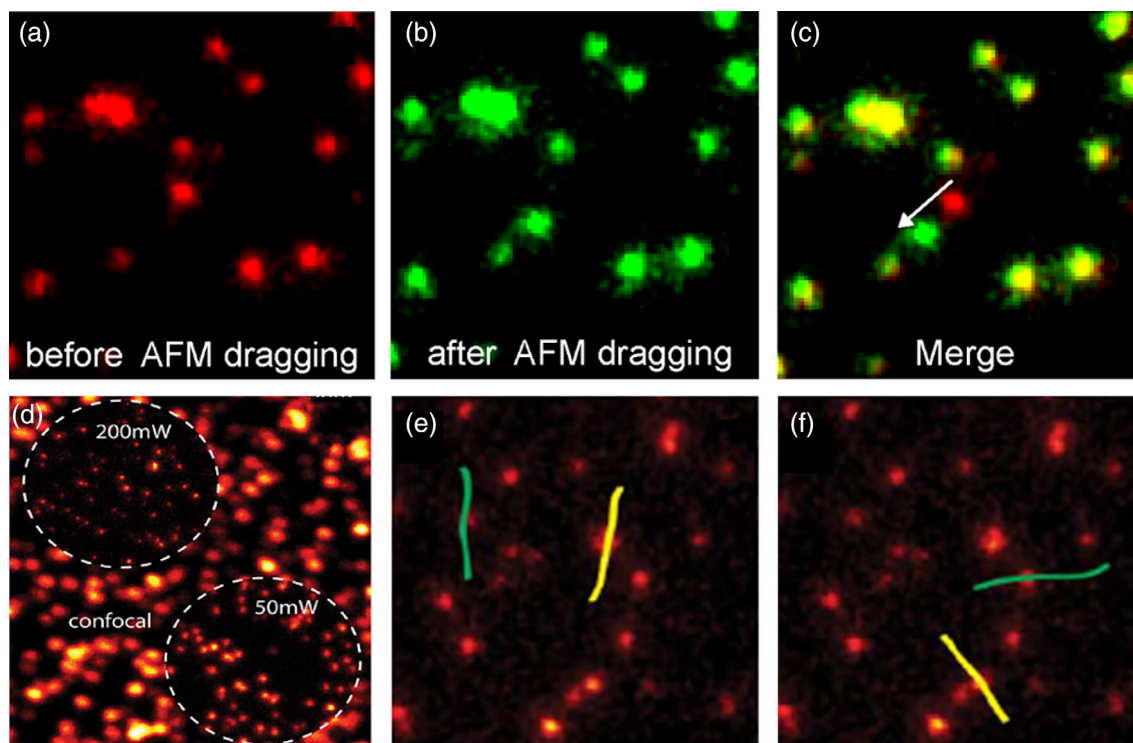


FIGURE 5 Nanomanipulation of fluorescent spheres of 40 nm size. (a,b) Stimulated emission depletion (STED) images of fluorescent beads before and after atomic force microscopy (AFM) dragging at the same area, respectively. (c) Merged image of STED images. (d) Confocal image of beads with two different STED views to show the enhanced resolution image representing the effect of reduced STED power used for conducting AFM manipulation. (e,f) Two manipulation line patterns in the AFM software for each STED and confocal imaging modes, respectively. The image has been modified from Chacko, Canale, Härke, and Diaspro (2013)

In 2017, Curry et al. carried out AFM–STED microscopy on living labeled astrocytes to directly compare super-resolved fluorescence images of cytoskeletal organization with membrane mechanical properties under normal conditions, or during migration *in vitro*. This further step toward the study of living systems represents a crucial milestone in AFM–super-resolution correlative microscopy (Curry, Ghézali, Kaminski Schierle, Rouach, & Kaminski, 2017). From AFM topography images, they found out that actin networks are highly organized in arrays of fibers, and play an important role in membrane stiffness. In addition, the AFM probe resolved a polarized distribution of actin filaments in the height images within *in vitro* astrocytes. They showed that polarized migration correlates with changes in membrane stiffness likely to promote focal adhesion complexes, contraction, and growth of fine astroglial protrusions. On the other hand, they demonstrated that microtubule filaments imaged with STED did not correlate with the astrocyte topography visualized by AFM (Figure 6). They observed microtubules do not have such specific organized and polarized structures, and they do not contribute significantly to the astrocyte stiffness. Their results were in agreement with other studies carried out in different cell types representing a fine interplay between cellular elasticity and actin network.

Cosentino, Canale, Bianchini, and Diaspro (2019) performed correlative AFM–STED measurements to study amyloid aggregates formation starting from different monomeric peptides (Figure 7). In

particular, the authors investigated the *in vitro* aggregation of insulin, a nonpathological peptide, and two alloforms of β amyloid peptides ($A\beta$), a molecule responsible for the neurodegenerative process in Alzheimer's disease. In particular, they targeted mature insulin fibrils formed after 14 days of incubation in denaturing conditions (Figure 7b–d). Only a fraction of the monomers involved in the aggregation process were labeled. They used different dye-to-protein ratios: 1:20, 1:100, and 1:500. The presence of fluorophores not only decreased the kinetics of the aggregation, a very well-known effect, but also bolded the coexistence of labeled and unlabeled fibrils. This phenomenon was still unknown and revealed a particular mechanism induced by the presence of the fluorescence tag. From already published data, they found that at least at the dye-to-protein ratio of 1:20 and 1:100, the number of fluorescent peptides was sufficient to have all fluorescent aggregates, in the case of a stochastic process of aggregation, in which the labeled monomers distributed homogeneously in the fibrils. The results suggested the coexistence of different aggregation pathways. Labeled molecules can follow just some of these pathways. They observed that the fibrils thickness at different dye-to-protein ratios does not change within the experimental errors, although the unlabeled fibrils are slightly thinner, likely due to a steric effect or a different organization of the protofilaments within the fibrillar aggregates. However, clear structural diversity between fluorescent, or dark fibrils was not detected. The same mechanism was

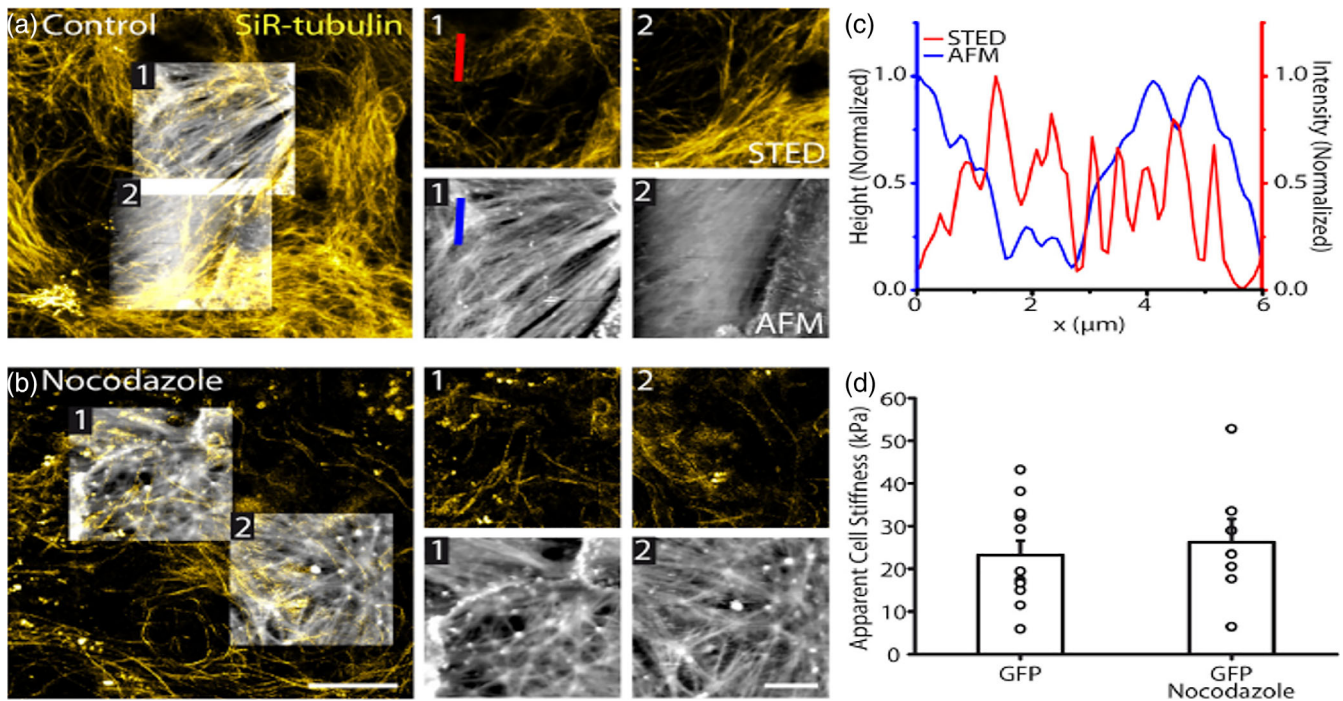


FIGURE 6 Stimulated emission depletion (STED)–atomic force microscopy (AFM) imaging of live astrocytes to correlate the spatial distribution of labeled cytoskeletal elements with cell morphology and membrane stiffness. (a) STED image of labeled tubulin overlaid with AFM images taken in scan areas 1 and 2. Tubulin filaments imaged with AFM show different orientation compared to the corresponding STED images (AFM: 32.2°, STED: 51.3°; region 2: AFM: 29.0°, STED: 40.0°). (b) Line profile of height (AFM) and intensity (STED) indicated in the area of interest showing incompatibility in some locations of picks. (c) STED image of labeled tubulin which has been depolymerized by nocodazole (16 mM, 1 hr) overlaid with AFM images taken in scan area 1 and 2. (d) Bar graph represents Cell labeling with nocodazole which has no significant effect on cell stiffness ($n = 7, p > .05$, Mann–Whitney test). Scale bars are 10 mm (large images) and 5 mm (zoomed images). Figure from Curry et al. (2017)

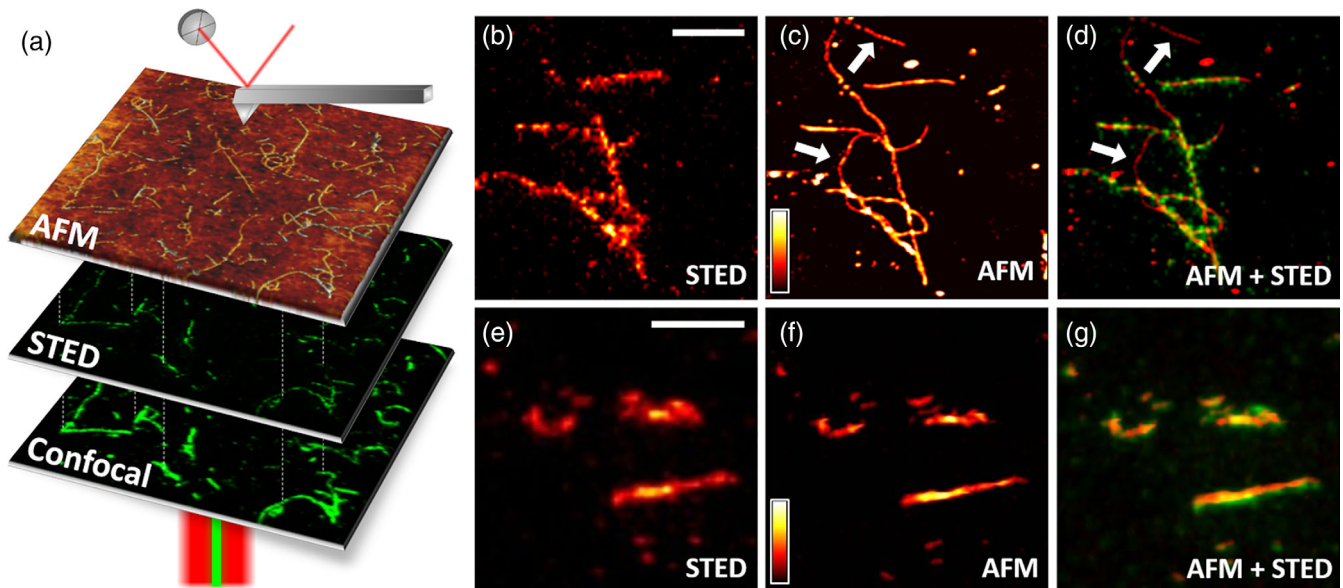


FIGURE 7 Confocal laser scanning microscope (CLSM) and stimulated emission depletion (STED) microscopy are inspecting the sample from below, shining the laser through the transparent glass substrate, while the atomic force microscopy (AFM) tip is scanning the sample from above, moving in the liquid environment of the AFM fluid chamber (a). STED (b) and AFM (c) images are acquired on the same area, and after applying a calibration procedure to eliminate the optical aberration from the STED image are overlapped (d). The with arrow in (c) and (d) indicated two aggregates that are present only in the AFM image. Immunolabeled fibrils are all displayed with both techniques (e,f) as demonstrated by the high correlation between the two images (g). Scale bars: 1 μm

also demonstrated for $A\beta 1-42$ and $A\beta 1-40$ fibrils, suggesting a general protein aggregation mechanism. The authors showed that by applying immunolabeling on preformed fibrils (Figure 7e–g), all the aggregates appeared on both AFM and STED imaging demonstrating that the loss of fluorescence is not due to an instrumental bias, but is inherently related to the process of sample formation. This work provides evidence of a fundamental drawback in fluorescence microscopy. Unexpected phenomena could take place, induced by the structural changes induced in the molecules.

Furthermore, labeling can fail for an unknown reason. Fluorescence microscopy cannot highlight all these anomalies, but only the coupling with a second high-resolution and label free technique, such as AFM, can reveal them. This work generates a warning for all the fluorescence users: a deeper control for possible artifacts induced by the fluorophore is needed. This will probably be an essential issue for the future development of the technique. Furthermore, it indicates how AFM can complement fluorescence microscopy in an AFM-assisted fluorescence microscopy mode.

2.3.2 | AFM–SMLM

Chacko, Zanicchi, and Diaspro (2013) also worked at the coupling between AFM and STORM, demonstrating the strength of correlative STORM-AFM recordings toward resolving the cytoskeletal structures, such as microtubule filaments. It is known that the topology gets difficult to be interpreted in a thick sample. They visualized this fact through 3D rendered view of z stack image of microtubule structure. In this case, 3D STORM imaging capabilities could represent a better overlay of information from the external layer of the cell provided by the two imaging modalities, and the multicolor imaging could separate different types of proteins from the unspecific AFM topology (Chacko, Zanicchi, & Diaspro, 2013). It is interesting to note that, in some cases, part of the sample displayed in the AFM image is not visible in the fluorescence image. This fact suggested a new vision: not only the optical image could complement the AFM signal, adding specificity, but also the unlabeled AFM image could help to reveal the presence of feature completely invisible by fluorescence; this issue

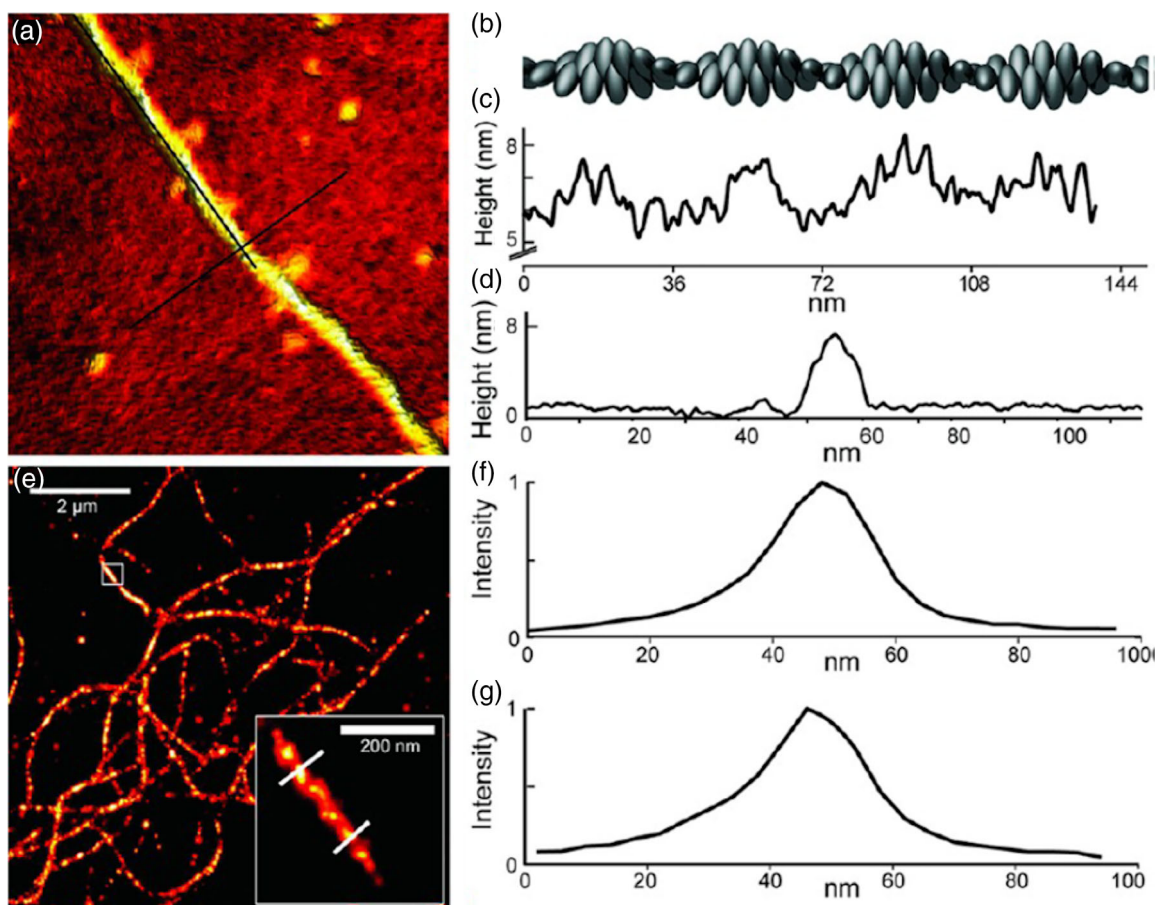


FIGURE 8 Imaging polymerized actin filaments deposited on a glass coverslip using correlated atomic force microscopy (AFM)–dSTORM microscopy. (a) AFM image of Actin filaments ($200 \text{ nm} \times 200 \text{ nm}$) revealing the $\sim 36 \text{ nm}$ periodicity of its helical structure which has been shown as 3D model in (b), as well. (c) Height profile of Actin filaments obtained by AFM along the filament (profile line indicated in (a)). (d) Cross-sectional profile with full-width at half-maximum (FWHM) height of about 10 nm corresponds to height analysis obtained by AFM. (e) dSTORM image of F-actin labeled with phalloidin-alexa647 with a zoomed area. Scale bars are $2 \mu\text{m}$ (large image) and 200 nm (zoomed image). (f, g) Intensity profiles related to the lines in the zoomed area, normalized to the maximum intensity of the profile that have a cross section with an FWHM of $\sim 24 \text{ nm}$. Figure from Odermatt et al. (2015)

was focused in more details some years later by Cosentino et al. (2019), in the work described in the previous section. A few months later, Monserrate, Casado, and Flors (2014) showed an overlapped image of λ -DNA filaments labeled with YOYO-1. The authors used the new possibility offered by correlative microscopy to find the best parameters optimizing the balance between spatial resolution and localization density, reinforcing the idea of AFM-assisted super-resolution imaging.

AFM imaging in correlative microscopy is generally affected by the mechanical noise, due to the presence of vibrations generated by the presence of several components with their noisy cooling system. Odermatt et al. (2015) designed a correlated system coupling single molecule localization microscopy setup (STORM and PALM) with AFM. The peculiarity of this design was the lack of mechanical contact between the support structure that holds the AFM and the optical microscope body. This particular design was created to reduce the mechanical noise induced on the AFM probe, aiming at limiting one of the main drawback inherently related to correlative microscopy. To prove the true performance of the system, the authors operated dSTORM-AFM to directly visualize labeled polymerized actin filaments deposited on a glass coverslip coated with APTES ((3-aminopropyl)triethoxysilane) (Figure 8). First, the monomers in actin filaments were labeled by phalloidin-Alexa647 for the correlative experiment. The 3D imaging capability of both techniques revealed the helical structure of F-actin. In this case, the height of actin filaments obtained by AFM was between 6 and 8 nm with a full-width at half-maximum (FWHM) of about 10 nm. The FWHM of dSTORM was 24 nm with a mean photon count of about 5,500 and a mean localization precision of 12.5 nm for the filament bundles. Since Alexa647 emission deteriorates after exposure to the AFM laser, phalloidin-Atto488 was used instead to label F-actin. This significantly reduced the bleaching of the dye, but also reduced the photon count, and therefore the ultimately achievable localization precision. In this case, the height and width of the actin filament bundles measured by AFM were 14 and 65 nm FWHM, respectively. The FWHM of dSTORM was 94 nm and of TIRF 271 nm for the filament bundles. Comparing the width of the actin bundles as measured by AFM and by dSTORM, they found that dSTORM provides comparable values to AFM. Besides, they observed a correlation between the height of F-actin and the number of localizations. This result suggested that the fluctuation of localization densities is partially due to the presence of actin bundles rather than single filaments likely contributing to the local differences of localizations recorded by dSTORM along the filament. All these sets of experiments demonstrated the ability for the setup to minimize the mechanical noise transmitted to the AFM, hence improving the AFM performances.

3 | CONCLUSION

In the last decade, correlative microscopy has become an essential tool for advanced investigation (Smith, 2012). The correlation between AFM and optical microscopy has achieved a prominent role

in biological research, thanks to the two instruments ability to work on living/dynamic systems in their native conditions. The way that leads from the first pioneering attempts to the modern applications involving super-resolution optical microscopy has been 20 years long. Here, we showed the fundamental steps of this path. Furthermore, we focused on the most important results obtained in the last years. The improvement of the integration level between the two microscopes will enable even more sophisticated analysis. Also, the possibility of finding a more user-friendly and commercially available integrated system could significantly enhance the diffusion of this technique in biological and biomedical research.

ORCID

Claudio Canale  <https://orcid.org/0000-0002-7582-6849>

REFERENCES

- Bellani, S., Mescola, A., Ronzitti, G., Tsumahima, H., Tilve, S., Canale, C., ... Chiergatti, E. (2014). GRP78 clustering at the cell surface of neurons transduces the action of exogenous alpha-synuclein. *Cell Death and Differentiation*, 21(12), 1971–1983. <https://doi.org/10.1038/cdd.2014.111>.
- Binnig, G., Quate, C. F., & Gerber, C. (1986). Atomic force microscope. *Physical Review Letters*, 56(9), 930–933.
- Chacko, J. V., Canale, C., Harke, B., & Diaspro, A. (2013). Sub-diffraction nano manipulation using STED AFM. *PLoS One*, 8(6), e66608.
- Chacko, J. V., Harke, B., Canale, C., & Diaspro, A. (2014). Cellular level nanomanipulation using atomic force microscope aided with super-resolution imaging. *Journal of Biomedical Optics*, 19(10), 1.
- Chacko, J. V., Zancacchi, F. C., & Diaspro, A. (2013). Probing cytoskeletal structures by coupling optical superresolution and AFM techniques for a correlative approach. *Cytoskeleton*, 70(11), 729–740.
- Cosentino, M., Canale, C., Bianchini, P., & Diaspro, A. (2019). AFM-STED correlative nanoscopy reveals a dark side in fluorescence microscopy imaging. *Science Advances*, 5(6), eaav8062.
- Curry, N., Ghézali, G., Kaminski Schierle, G. S., Rouach, N., & Kaminski, C. F. (2017). Correlative STED and atomic force microscopy on live astrocytes reveals plasticity of cytoskeletal structure and membrane physical properties during polarized migration. *Frontiers in Cellular Neuroscience*, 11, 104. <https://doi.org/10.3389/fncel.2017.00104>
- Di Bucchianico, S., Poma, A. M., Giardi, M. F., di Leandro, L., Valle, F., Biscarini, F., & Botti, D. (2011). Atomic force microscope nanolithography on chromosomes to generate single-cell genetic probes. *Journal of Nanobiotechnology*, 9(1), 27.
- Di Gaetano, S., Guglielmi, F., Arciello, A., Mangione, P., Monti, M., Pagnozzi, D., ... Piccoli, R. (2006). Recombinant amyloidogenic domain of ApoA-I: Analysis of its fibrillogenic potential. *Biochemical and Biophysical Research Communications*, 351(1), 223–228.
- Dickson, R. M., Cubitt, A. B., Tsien, R. Y., & Moerner, W. E. (1997). On/off blinking and switching behaviour of single molecules of green fluorescent protein. *Nature*, 388(6640), 355–358.
- Doss, B. L., Pan, M., Gupta, M., Grecni, G., Mège, R.-M., Lim, C. T., ... Ladoux, B. (2020). Cell response to substrate rigidity is regulated by active and passive cytoskeletal stress. *Proceedings of the National Academy of Sciences*, 117(23), 12817–12825.
- Dubremetz, J. F. (1998). Host cell invasion by *Toxoplasma gondii*. *Trends in Microbiology*, 6(1), 27–30.
- Dvorak, J. A., & Nagao, E. (1998). Kinetic analysis of the mitotic cycle of living vertebrate cells by atomic force microscopy. *Experimental Cell Research*, 242(1), 69–74.
- Eggeling, C., Ringemann, C., Medda, R., Schwarzmann, G., Sandhoff, K., Polyakova, S., ... Hell, S. W. (2009). Direct observation of the

- nanoscale dynamics of membrane lipids in a living cell. *Nature*, 457 (7233), 1159–1162.
- Ferrera, D., Canale, C., Marotta, R., Mazzaro, N., Gritti, M., Mazzanti, M., ... Gasparini, L. (2014). Lamin B1 overexpression increases nuclear rigidity in autosomal dominant leukodystrophy fibroblasts. *The FASEB Journal*, 28(9), 3906–3918.
- Garcia-Manyes, S., Redondo-Morata, L., Oncins, G., & Sanz, F. (2010). Nanomechanics of lipid bilayers: Heads or tails? *Journal of the American Chemical Society*, 132(37), 12874–12886.
- Haga, H., Sasaki, S., Kawabata, K., Ito, E., Ushiki, T., & Sambongi, T. (2000). Elasticity mapping of living "broblasts" by AFM and immunofluorescence observation of the cytoskeleton. *Ultramicroscopy*, 82, 253–258.
- Hansma, P., Elings, V., Marti, O., & Bracker, C. (1988). Scanning tunneling microscopy and atomic force microscopy: Application to biology and technology. *Science*, 242(4876), 209–216.
- Harke, B., Chacko, J. V., Haschke, H., Canale, C., & Diaspro, A. (2012). A novel nanoscopic tool by combining AFM with STED microscopy. *Optical Nanoscopy*, 1(1), 3.
- Hell, S. W., & Wichmann, J. (1994). Breaking the diffraction resolution limit by stimulated emission: Stimulated-emission-depletion fluorescence microscopy. *Optics Letters*, 19(11), 780.
- Henderson, E., & Sakaguchi, D. S. (1993). Imaging F-actin in fixed glial cells with a combined optical fluorescence/atomic force microscope. *NeuroImage*, 1(2), 145–150.
- Hess, S. T., Girirajan, T. P. K., & Mason, M. D. (2006). Ultra-high resolution imaging by fluorescence photoactivation localization microscopy. *Biophysical Journal*, 91(11), 4258–4272.
- Jonkman, J., Brown, C. M., Wright, G. D., Anderson, K. I., & North, A. J. (2020). Tutorial: Guidance for quantitative confocal microscopy. *Nature Protocols*, 15(5), 1585–1611.
- Kolodny, L. A., Willard, D. M., Carillo, L. L., Nelson, M. W., & van Orden, A. (2001). Spatially correlated fluorescence/AFM of individual nanosized particles and biomolecules. *Analytical Chemistry*, 73(9), 1959–1966.
- Kondra, S., Laishram, J., Ban, J., Migliorini, E., Di Foggia, V., Lazzarino, M., ... Ruaro, M. E. (2009). Integration of confocal and atomic force microscopy images. *Journal of Neuroscience Methods*, 177(1), 94–107.
- Kruger, D. H., Schneck, P., & Gelderblom, H. R. (2000). Helmut Ruska and the visualisation of viruses. *The Lancet*, 355, 5.
- Liu, Z., Lavis, L. D., & Betzig, E. (2015). Imaging live-cell dynamics and structure at the single-molecule level. *Molecular Cell*, 58(4), 644–659.
- Medalsy, I., Hensen, U., & Muller, D. J. (2011). Imaging and quantifying chemical and physical properties of native proteins at molecular resolution by force-volume AFM. *Angewandte Chemie, International Edition*, 50(50), 12103–12108.
- Mescola, A., Vella, S., Scotto, M., Gavazzo, P., Canale, C., Diaspro, A., ... Vassalli, M. (2012). Probing cytoskeleton organisation of neuroblastoma cells with single-cell force spectroscopy: Probing cytoskeleton of neuroblastoma cells with SCFS. *Journal of Molecular Recognition*, 25(5), 270–277.
- Monserate, A., Casado, S., & Flors, C. (2014). Correlative atomic force microscopy and localization-based super-resolution microscopy: Revealing labelling and image reconstruction artefacts. *ChemPhysChem*, 15(4), 647–650.
- Odermatt, P. D., Shivanandan, A., Deschout, H., Jankele, R., Nievergelt, A. P., Feletti, L., ... Fantner, G. E. (2015). High-resolution correlative microscopy: Bridging the gap between single molecule localization microscopy and atomic force microscopy. *Nano Letters*, 15 (8), 4896–4904.
- Putman, C. A. J., van der Werf, K. O., de Grooth, B. G., van Hulst, N. F., Segerink, F. B., & Greve, J. (1992). Atomic force microscope featuring an integrated optical microscope. *Ultramicroscopy*, 42–44, 1549–1552.
- Putman, C. A. J., van Leeuwen, A. M., de Grooth, B. G., Radosevic, K., & Greve, J. (1993). Atomic force microscopy combined with confocal laser scanning microscopy: A new look at cells. *Bioimaging*, 1, 63–70.
- Radmacher, M., Eberle, K., & Gaub, H. E. (1992). An AFM with integrated micro-fluorescence optics: Design and performance. *Ultramicroscopy*, 42–44, 968–972.
- Rayan, G., Guet, J.-E., Taulier, N., Pincet, F., & Urbach, W. (2010). Recent applications of fluorescence recovery after photobleaching (FRAP) to membrane bio-macromolecules. *Sensors*, 10(6), 5927–5948.
- Ross, J. A., & Jameson, D. M. (2008). Time-resolved methods in biophysics. 8. Frequency domain fluorometry: Applications to intrinsic protein fluorescence. *Photochemical & Photobiological Sciences*, 7(11), 1301.
- Rust, M. J., Bates, M., & Zhuang, X. (2006). Sub-diffraction-limit imaging by stochastic optical reconstruction microscopy (STORM). *Nature Methods*, 3(10), 793–796.
- Sanderson, M. J., Smith, I., Parker, I., & Bootman, M. D. (2014). Fluorescence microscopy. *Cold Spring Harbor Protocols*, 2014(10), pdb.top071795.
- Seghezza, S., Dante, S., Diaspro, A., & Canale, C. (2015). High resolution nanomechanical characterization of multi-domain model membranes by fast force volume: Nanomechanical characterization of multi-domain membranes by fast FV. *Journal of Molecular Recognition*, 28 (12), 742–750.
- Sheppard, C. J. R. (2017). Resolution and super-resolution. *Microscopy Research & Technique*, 80(6), 9. <https://doi.org/10.1002/jemt.22834>
- Smith, C. (2012). Two microscopes are better than one. *Nature*, 492(7428), 293–297.
- Swift, J. A., & Brown, A. C. (1970). An environmental cell for the examination of wet biological specimens at atmospheric pressure by transmission scanning electron microscopy. *Journal of Physics E*, 3(11), 924–926.
- Trucco, E., & Verri, A. (1998). *Introductory techniques for 3-D computer vision*. Upper Saddle River, NJ: Prentice Hall.
- Tychinsky, V. P., & Tikhonov, A. N. (2010). Interference microscopy in cell biophysics. 1. Principles and methodological aspects of coherent phase microscopy. *Cell Biochemistry and Biophysics*, 58(3), 107–116.
- Verschueren, H. (1985). Interference reflection microscopy in cell biology: Methodology and applications. *Journal of Cell Science*, 75(1), 279–301.
- Wallrabe, H., & Periasamy, A. (2005). Imaging protein molecules using FRET and FLIM microscopy. *Current Opinion in Biotechnology*, 16(1), 19–27.

How to cite this article: Jadavi S, Bianchini P, Cavalleri O, Dante S, Canale C, Diaspro A. Correlative nanoscopy: A multimodal approach to molecular resolution. *Microsc Res Tech*. 2021;84:2472–2482. <https://doi.org/10.1002/jemt.23800>